hep-ph/0409279
USM–TH–136
SLAC–PUB–9677
September 2004
Revised

Nuclear Antishadowing in Neutrino Deep Inelastic Scattering*

Stanley J. Brodsky [†a], **Ivan Schmidt**[‡b], **Jian-Jun Yang**[§b,c,d]

[a]Stanford Linear Accelerator Center, Stanford University,
Stanford, California 94309,
[b]Departamento de Física, Universidad Técnica Federico Santa María,
Casilla 110-V, Valparaíso, Chile
[c]Institut für Theoretische Physik, Universität Regensburg,
D-93040 Regensburg, Germany,
[d]Department of Physics, Nanjing Normal University,
Nanjing 210097, China

*Work supported in part by the Department of Energy under contract number DE–AC02–76SF00515, by the Foundation for University Key Teacher by the Ministry of Education (China), by Fondecyt (Chile) grant 1030355, and by the National Natural Science Foundation of China under Grant Numbers 19875024 and 10025523.

†e-mail:sjbth@SLAC.Stanford.EDU
‡e-mail: ivan.schmidt@fis.utfsm.cl
§deceased

Abstract

The shadowing and antishadowing of nuclear structure functions in the Gribov-Glauber picture is due respectively to the destructive and constructive interference of amplitudes arising from the multiple-scattering of quarks in the nucleus. The effective quark-nucleon scattering amplitude includes Pomeron and Odderon contributions from multi-gluon exchange as well as Reggeon quark-exchange contributions. We show that the coherence of these multiscattering nuclear processes leads to shadowing and antishadowing of the electromagnetic nuclear structure functions in agreement with measurements. This picture leads to substantially different antishadowing for charged and neutral current reactions, thus affecting the extraction of the weak-mixing angle θ_W. We find that part of the anomalous NuTeV result for θ_W could be due to the nonuniversality of nuclear antishadowing for charged and neutral currents. Detailed measurements of the nuclear dependence of individual quark structure functions are thus needed to establish the distinctive phenomenology of shadowing and antishadowing and to make the NuTeV results definitive.

1 Introduction

The precise determination of the weak-mixing angle $\sin^2\theta_W$ plays a crucial role in testing the standard model of electroweak interactions. Until recently, a consistent value was obtained from all of the electroweak observables [1]. However, the NuTeV Collaboration [2] has determined a value for $\sin^2\theta_W$ from measurements of the ratio of charged and neutral current deep inelastic neutrino–nucleus and anti-neutrino–nucleus scattering in iron targets which has a 3σ deviation with respect to the fit of the standard model predictions from other electroweak measurements [1]. This contrasts with the recent determination of $\sin^2\theta_W$ from parity violation in Möller scattering which is consistent with the standard model [3]. Although the NuTeV analysis takes into account many sources of systematic errors, there still remains the question of whether the reported deviation could be accounted for by QCD effects such as the asymmetry of the strange-antistrange quark sea [4, 5] or other Standard Model effects [6, 7, 8, 9, 10, 11, 12, 13, 14, 15, 16]. In this paper we shall investigate whether the anomalous NuTeV result for $\sin^2\theta_W$ could be due to the different behavior of leading-twist nuclear shadowing and antishadowing effects for charged and neutral currents.

The physics of the nuclear shadowing in deep inelastic scattering can be most easily understood in the laboratory frame using the Glauber-Gribov picture [17, 18]. The virtual photon, W or Z^0 produces a quark-antiquark color-dipole pair which can interact diffractively or inelastically on the nucleons in the nucleus. The destructive interference of diffractive amplitudes from pomeron exchange on the upstream nucleons then causes shadowing of the virtual photon interactions on the back-face nucleons [19, 20, 21, 22, 23, 24]. As emphasized by Ioffe [21], the coherence between processes which occur on different nucleons at separation L_A requires small Bjorken $x_B : 1/Mx_B = 2\nu/Q^2 \geq L_A$. The coherence between different quark processes is also the basis of saturation phenomena in DIS and other hard QCD reactions at small x_B [25], and coherent multiple parton scattering has been used in the analysis of $p + A$ collisions in terms of the perturbative QCD factorization approach [26]. An example of the interference of one- and two-step processes in deep inelastic lepton-

nucleus scattering illustrated in Fig. 1.

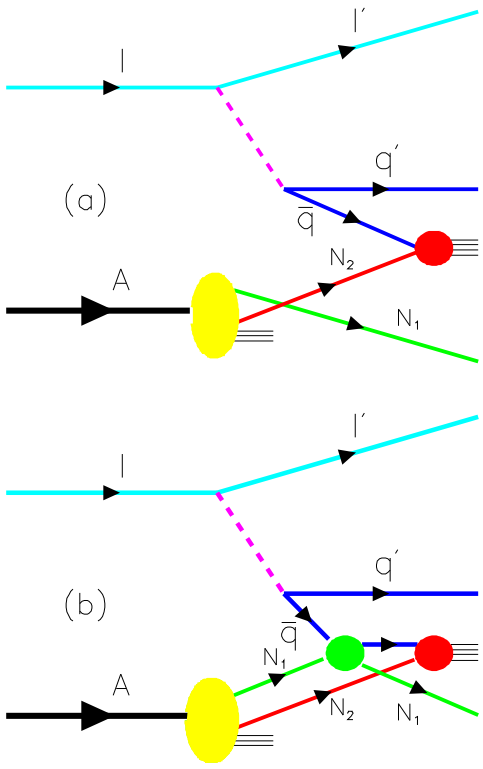

Figure 1: The one-step and two-step processes in DIS on a nucleus. If the scattering on nucleon N_1 is via pomeron exchange, the one-step and two-step amplitudes are opposite in phase, thus diminishing the $\overline{q}$ flux reaching N_2. This causes shadowing of the charged and neutral current nuclear structure functions.

An important aspect of the shadowing phenomenon is that the diffractive contribution $\gamma^* N \to XN'$ to deep inelastic scattering (DDIS) where the nucleon N_1 in Fig. 1 remains intact is a constant fraction of the total DIS rate, confirming that it is a leading-twist contribution. The Bjorken scaling of DDIS has been observed at HERA [27, 28, 29]. As shown in Ref. [30], the leading-twist contribution to DDIS arises in QCD in the usual parton model frame when one includes the nearly instantaneous gluon exchange final-state interactions of the struck quark with the target spectators. The same final state interactions also lead to leading-twist single-spin asymmetries in semi-inclusive DIS [31]. Thus the shadowing of nuclear structure functions is also a leading-twist effect.

It was shown in Ref. [32] that if one allows for Reggeon exchanges which leave a nucleon intact, then one can obtain *constructive* interference among the multi-scattering amplitudes in the nucleus. A Bjorken-scaling contribution to DDIS from Reggeon exchange has in fact also been observed at HERA [28, 29]. The strength and energy dependence of the $C = +$ Reggeon $t-$channel exchange contributions to virtual Compton scattering is constrained by the Kuti-Weisskopf [33] behavior $F_2(x) \sim x^{1-\alpha_R}$ of the non-singlet electromagnetic structure functions at small x. The phase of the Reggeon exchange amplitude is determined by its signature factor. Because of this complex phase structure [32], one obtains constructive interference and *antishadowing* of the nuclear structure functions in the range $0.1 < x < 0.2$ – a pronounced excess of the nuclear cross section with respect to nucleon additivity [34].

In the case where the diffractive amplitude on N_1 is imaginary, the two-step process has the phase $i \times i = -1$ relative to the one-step amplitude, producing destructive interference. (The second factor of i arises from integration over the quasi-real intermediate state.) In the case where the diffractive amplitude on N_1 is due to $C = +$ Reggeon exchange with intercept $\alpha_R(0) = 1/2$, for example, the phase of the two-step amplitude is $\frac{1}{\sqrt{2}}(1-i) \times i = \frac{1}{\sqrt{2}}(i+1)$ relative to the one-step amplitude, thus producing constructive interference and antishadowing. This is discussed in more detail in the following sections.

Odderon exchange due to three-gluon exchange leads to an elastic quark-nucleon amplitude which is nearly real in phase, thus providing an additional mechanism for antishadowing. We shall show that the combination of Pomeron, Reggeon, and Odderon exchanges in multi-step processes leads to shadowing and antishadowing of the electromagnetic nuclear structure functions in agreement with measurement in electromagnetic interactions. Shadowing of the nuclear structure functions is thus due to the dynamics of $\gamma^* A$ interactions; it is not a property of the nuclear light-front wavefunction computed in isolation [30].

Evidence for the Odderon has been illusive; a detailed discussion can be found in a recent review by Ewerz [35]. A clear signal appears in the difference of proton-proton vs. proton anti-proton scattering. From the perspective of QCD, the Odderon represents the color-singlet effects of three gluons in the $t-$channel. A general treatment in

the context of the BFKL program has been given by Bartels, Lipatov, and Vacca [36] The Odderon has Regge intercept $\alpha_{\mathcal{O}} \sim 1$, $C = -$, and thus its phase is nearly pure real. The Odderon does not contribute directly to the structure functions since it gives a real contribution to the virtual Compton amplitude. However, it can play an important role in the multi-scattering series in the nuclear target.

There can be other important antishadowing mechanisms. Processes which can occur on a nucleus, but are forbidden on a nucleon, will enhance the nuclear structure functions. For example, pseudoscalar Reggeon exchange amplitudes do not contribute to DIS on a nucleon target since the helicity-conserving forward amplitude $\gamma^* N \to \gamma^* N$ vanishes at $t = 0$. However in the nuclear case, the interactions of the scattered quark (due to pomeron exchange) on a second nucleon N_2 in a nuclear target can skew the kinematics of $\gamma^* N_1 \to \gamma^* N_1'$, thus allowing the pseudoscalar exchange to occur on the nucleon N_1 at $t \neq 0$. This also requires nonzero orbital angular momentum of the nucleons in the nuclear wavefunction. Notice that the virtual Compton amplitude on the nucleus $\gamma^* A \to \gamma^* A$ is still evaluated at zero momentum transfer $t = 0$. Thus in general one should include pseudoscalar exchange in the parametrization of the quark multiple scattering processes.

In Fig. 2 we illustrate several leading-twist QCD contributions to the nuclear structure function as calculated from the absorptive part of the forward virtual Compton amplitude $Im\, T(\gamma^* A \to \gamma^* A)$, in the $q^+ = 0, q_\perp^2 = Q^2$ parton model frame and in the laboratory frame where $q^+ > 0$. Notice the final-state two-gluon exchange "pomeron" interaction of the outgoing quark on a target neutron. Figure 2 (c) is an illustration of a doubly inelastic discontinuity of the same two-step process as (a) in the laboratory frame $q^+ > 0$. The $u\overline{u}$ fluctuation of the virtual photon first scatters inelastically on a neutron via a single gluon exchange which produces an excited color state 8_C of the neutron. This is then followed by the annihilation of the $\overline{u}$ quark on a proton. The two-step amplitudes of (b) or (c) will interfere destructively with the single-step annihilation amplitude on the proton alone, thus producing shadowing. If the proton spin S_z^p is flipped ($\lambda' \neq \lambda$) by the valence interaction, as occurs in pseudoscalar Reggeon exchange, then the single-step process cannot contribute to the forward vir-

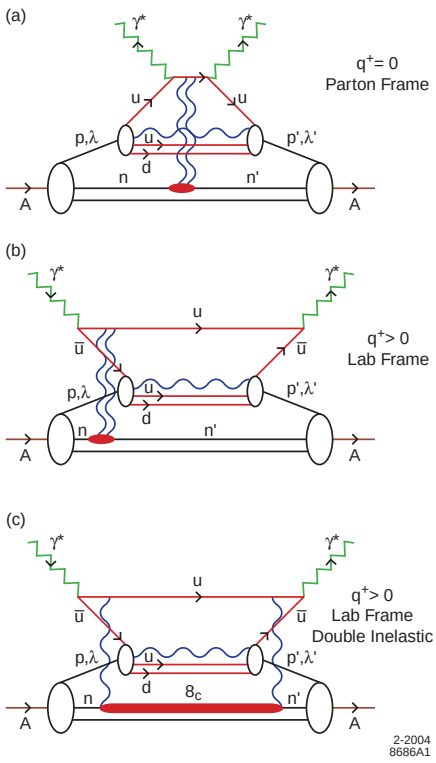

Figure 2: Representation of leading-twist QCD contributions to the nuclear structure function as calculated from the absorptive part of the forward virtual Compton amplitude $Im\, T(\gamma^* A \to \gamma^* A)$. (a) Illustration of a two-step contribution in the usual $q^+ = 0, q_\perp^2 = Q^2$ parton model frame. The deep inelastic scattering of a lepton on a valence quark of a target proton is followed by the final-state two-gluon exchange "pomeron" interaction of the outgoing quark on a neutron. (b) Illustration of the physics of the same two-step process illustrated in (a), but in the laboratory frame where $q^+ > 0$. The $u\overline{u}$ fluctuation of the virtual photon scatters elastically via two-gluon exchange on a neutron; this is then followed by the annihilation of the $\overline{u}$ quark on a proton. (c) Illustration of a doubly inelastic discontinuity of the same two-step process as (a) in the laboratory frame $q^+ > 0$. The $u\overline{u}$ fluctuation of the virtual photon first scatters inelastically on a neutron via a single-gluon exchange which produces an excited color state 8_C of the neutron. This is then followed by the annihilation of the $\overline{u}$ quark on a proton.

tual Compton amplitude, and the two-step process itself produces antishadowing of the valence quark distributions. Similar processes occur in the case of the electroweak currents.

Figure 3 illustrates a similar situation, but for the three-gluon "Odderon" exchange. In this case, the two-step amplitudes of (b) or (c) can interfere constructively with the Regge-behaved single-step annihilation amplitude on the proton alone, thus producing antishadowing. Similar processes occur in the case of the electroweak currents.

The Reggeon contributions to the quark scattering amplitudes depend specifically on the quark flavor; for example the isovector Regge trajectories couple differently to u and d quarks. The s and $\overline{s}$ couple to yet different Reggeons. This implies distinct antishadowing effects for each quark and antiquark component of the nuclear structure function; this in turn implies nonuniversality of antishadowing of the charged, neutral, and electromagnetic current. Anti-neutrino and neutrino reactions will also have different antishadowing effects. In addition, there is another source of antishadowing, specific to non-abelian theories, which is discussed in more detail in the appendix. It includes one-gluon exchange $\times$ Reggeon exchange, assuming the existence of hidden-color components in the nuclear wavefunction. We do not explicitly include this effect in our analysis since the parameterization is uncertain.

There are also antishadowing contributions arising from two-step processes involving Reggeon $\times$ Reggeon exchange, but these contributions are power-law suppressed in the Bjorken limit. We will not include these higher-twist effects in our analysis.

In this paper we shall show in detail that the Gribov-Glauber picture for nuclear deep inelastic scattering leads to substantially different nuclear effects for charged and neutral currents; in fact, the neutrino and antineutrino cross sections are each modified in substantially different ways due to the various allowed Regge exchanges. This non-universality of nuclear effects will modify the extraction of the weak-mixing angle $\sin^2\theta_W$ obtained from the ratio of charged and neutral current deep inelastic neutrino-nucleus scattering.

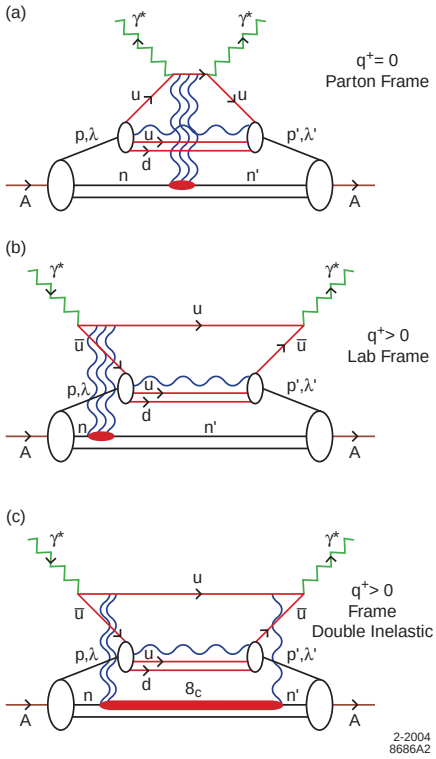

Figure 3: Representation of leading-twist QCD contributions to the nuclear structure function from the absorptive part of the forward virtual Compton amplitude $Im\, T(\gamma^* A \to \gamma^* A)$ involving odderon exchange. (a) Illustration of a two-step contribution in the $q^+ = 0, q_\perp^2 = Q^2$ parton model frame – deep inelastic lepton scattering on a valence quark of a target proton followed by the final-state three-gluon exchange "Odderon" interaction of the outgoing quark on a target neutron. (b) Illustration of the physics of the same two-step process shown in (a), but in the laboratory frame where $q^+ > 0$. The $u\overline{u}$ fluctuation of the virtual photon first scatters elastically via three-gluon exchange on a neutron; this is then followed by the annihilation of the $\overline{u}$ quark on a proton. (c) Illustration of a doubly inelastic discontinuity of the same two-step process as (a) in the laboratory frame $q^+ > 0$. The $u\overline{u}$ fluctuation of the virtual photon first scatters inelastically on a neutron via two-gluon exchange which produces an excited color state 8_C of the neutron. This is then followed by the annihilation of the $\overline{u}$ quark on a proton. The two-step amplitudes of (b) or (c) can interfere constructively with the Regge-behaved single-step annihilation amplitude on the proton alone, thus producing antishadowing. Similar processes occur in the case of the electroweak currents.

2 Nuclear shadowing and antishadowing effects due to multiple scattering

In this section, we will extend the analysis of Ref. [32] for the electromagnetic interaction case to the neutrino DIS case. The general approach is based on the "covariant parton model [37, 38], which provides a relationship of deep inelastic cross section to quark-nucleon scattering. The central idea is the following: In neutrino DIS on a nucleus A, although the virtual current may interact inelastically with a nucleon coming from the nucleus in a one-step process as shown in Fig. 1(a), it can also interact elastically with several nucleons before the final nucleon interacts inelastically as depicted in Fig. 1(b). The interacting antiquark or quark is spacelike:

$$\tau^2 = -k^2 = x(s + k_\perp^2)/(1 - x) - xM^2 + k_\perp^2 \tag{1}$$

is the negative of the invariant momentum squared of the interacting parton. Here $M = \frac{1}{2}(M_p + M_n)$ is the nucleon mass, and $k_\perp$ is the parton's transverse momentum. The quark-nucleon amplitude is assumed to be damped at large quark virtuality τ, so that the quark-nucleon invariant $s = (k + p)^2$ grows as $1/x$. This description of deep inelastic scattering is consistent with recent analysis of the role of final state gluon interactions in QCD when one chooses light-cone gauge to make the Wilson line integral vanish [30].

At high energies the phase of the elastic amplitude is approximately imaginary since it corresponds to Pomeron exchange. The accumulated phase in multiple scattering is also imaginary. Therefore, the two-step amplitude is coherent and opposite in phase to the one-step amplitude where the beam interacts directly on N_2 without initial-state interactions; the target nucleon N_2 feels less incoming flux, which results in nuclear shadowing. Since there may be an α_R Reggeon or Odderon contribution to the $\overline{q}N$ amplitude, the real phase introduced by such contributions leads to antishadowing effect. In this picture, antishadowing is attributed to a dynamical mechanism rather than being enforced to satisfy the momentum sum rule [39]. The sum rule can still be maintained by the nuclear modifications of the gluon distribution.

We now develop the detailed formulas which describe the nuclear shadowing and

antishadowing effects.

2.1 Parameterizations of quark-nucleon scattering

We shall assume that the high-energy antiquark-nucleon scattering amplitude $T_{\overline{q}N}$ has the Regge and analytic behavior characteristic of normal hadronic amplitudes. Following the model of Ref. [32], we consider a standard Reggeon at $\alpha_R = \frac{1}{2}$, an Odderon exchange term, a pseudoscalar exchange term, and a term at $\alpha_R = -1$, in addition to the Pomeron-exchange term.

The Pomeron exchange has the intercept $\alpha_P = 1 + \delta$. For the amputated $\overline{q} - N$ amplitude $T_{\overline{q}N}$ and $q - N$ amplitude T_{qN} with $q = u$, and d, $N = p$, and n, we assume the following parameterizations, including terms which represent pseudoscalar Reggeon exchange. Then resulting amplitudes are:

$$\begin{aligned} T_{\overline{u}-p} &= \sigma\Bigg[s\left(i + \tan\frac{\pi\delta}{2}\right)\beta_1(\tau^2) - s\beta_{\mathcal{O}}(\tau^2) - (1-i)s^{1/2}\beta_{1/2}^{0^+}(\tau^2) \\ &\quad +(1+i)s^{1/2}\beta_{1/2}^{0^-}(\tau^2) - (1-i)s^{1/2}\beta_{1/2}^{1^+}(\tau^2) + W(1-i)s^{1/2}\beta_{1/2}^{\rm pseudo}(\tau^2) \\ &\quad +(1+i)s^{1/2}\beta_{1/2}^{1^-}(\tau^2) + is^{-1}\beta_{-1}^{u}(\tau^2)\Bigg], \end{aligned} \tag{2}$$

$$\begin{aligned} T_{\overline{d}-p} &= \sigma[s\left(i + \tan\frac{\pi\delta}{2}\right)\beta_1(\tau^2) - s\beta_{\mathcal{O}}(\tau^2) - (1-i)s^{1/2}\beta_{1/2}^{0^+}(\tau^2) \\ &\quad +(1+i)s^{1/2}\beta_{1/2}^{0^-}(\tau^2) + (1-i)s^{1/2}\beta_{1/2}^{1^+}(\tau^2) + W(1-i)s^{1/2}\beta_{1/2}^{\rm pseudo}(\tau^2) \\ &\quad -(1+i)s^{1/2}\beta_{1/2}^{1^-}(\tau^2) + is^{-1}\beta_{-1}^{d}(\tau^2)], \end{aligned} \tag{3}$$

$$\begin{aligned} T_{u-p} &= \sigma\Bigg[s\left(i + \tan\frac{\pi\delta}{2}\right)\beta_1(\tau^2) + s\beta_{\mathcal{O}}(\tau^2) - (1-i)s^{1/2}\beta_{1/2}^{0^+}(\tau^2) \\ &\quad -(1+i)s^{1/2}\beta_{1/2}^{0^-}(\tau^2) - (1-i)s^{1/2}\beta_{1/2}^{1^+}(\tau^2) + W(1-i)s^{1/2}\beta_{1/2}^{\rm pseudo}(\tau^2) \\ &\quad -(1+i)s^{1/2}\beta_{1/2}^{1^-}(\tau^2)\Bigg], \end{aligned} \tag{4}$$

$$T_{d-p} = \sigma\Bigg[s\left(i + \tan\frac{\pi\delta}{2}\right)\beta_1(\tau^2) + s\beta_{\mathcal{O}}(\tau^2) - (1-i)s^{1/2}\beta_{1/2}^{0^+}(\tau^2) \tag{5}$$

$$-(1+i)s^{1/2}\beta^{0^-}_{1/2}(\tau^2)+(1-i)s^{1/2}\beta^{1^+}_{1/2}(\tau^2)+W(1-i)s^{1/2}\beta^{\rm pseudo}_{1/2}(\tau^2)$$
$$+(1+i)s^{1/2}\beta^{1^-}_{1/2}(\tau^2)\Bigg],$$

$$T_{\overline{u}-n} = \sigma\Bigg[s(i+\tan\frac{\pi\delta}{2})\beta_1(\tau^2)-s\beta_{\mathcal{O}}(\tau^2)-(1-i)s^{1/2}\beta^{0^+}_{1/2}(\tau^2) \quad (6)$$
$$+(1+i)s^{1/2}\beta^{0^-}_{1/2}(\tau^2)+(1-i)s^{1/2}\beta^{1^+}_{1/2}(\tau^2)+W(1-i)s^{1/2}\beta^{\rm pseudo}_{1/2}(\tau^2)$$
$$-(1+i)s^{1/2}\beta^{1^-}_{1/2}(\tau^2)+is^{-1}\beta^{d}_{-1}(\tau^2)\Bigg],$$

$$T_{\overline{d}-n} = \sigma\Bigg[s\left(i+\tan\frac{\pi\delta}{2}\right)\beta_1(\tau^2)-s\beta_{\mathcal{O}}(\tau^2)-(1-i)s^{1/2}\beta^{0^+}_{1/2}(\tau^2) \quad (7)$$
$$+(1+i)s^{1/2}\beta^{0^-}_{1/2}(\tau^2)-(1-i)s^{1/2}\beta^{1^+}_{1/2}(\tau^2)+W(1-i)s^{1/2}\beta^{\rm pseudo}_{1/2}(\tau^2)$$
$$+(1+i)s^{1/2}\beta^{1^-}_{1/2}(\tau^2)+is^{-1}\beta^{u}_{-1}(\tau^2)\Bigg],$$

$$T_{u-n} = \sigma\Bigg[s\left(i+\tan\frac{\pi\delta}{2}\right)\beta_1(\tau^2)+s\beta_{\mathcal{O}}(\tau^2)-(1-i)s^{1/2}\beta^{0^+}_{1/2}(\tau^2) \quad (8)$$
$$-(1+i)s^{1/2}\beta^{0^-}_{1/2}(\tau^2)++W(1-i)s^{1/2}\beta^{\rm pseudo}_{1/2}(\tau^2)$$
$$+(1-i)s^{1/2}\beta^{1^+}_{1/2}(\tau^2)+(1+i)s^{1/2}\beta^{1^-}_{1/2}(\tau^2)\Bigg],$$

$$T_{d-n} = \sigma\Bigg[s\left(i+\tan\frac{\pi\delta}{2}\right)\beta_1(\tau^2)+s\beta_{\mathcal{O}}(\tau^2)-(1-i)s^{1/2}\beta^{0^+}_{1/2}(\tau^2) \quad (9)$$
$$-(1+i)s^{1/2}\beta^{0^-}_{1/2}(\tau^2)-(1-i)s^{1/2}\beta^{1^+}_{1/2}(\tau^2)+W(1-i)s^{1/2}\beta^{\rm pseudo}_{1/2}(\tau^2)$$
$$-(1+i)s^{1/2}\beta^{1^-}_{1/2}(\tau^2)\Bigg].$$

$W = 0$ and 1, since the pseudoscalar term cannot act just once in the multiple scattering.

Here

$$\beta_j(\tau^2)=\frac{f_j}{1+(\tau^2/\overline{\nu}_j^2)^{n_j}} \quad (10)$$

with $j = 1,\ 1/2,\ -1,\ \mathcal{O}$ and *pseudo* (pseudoscalar). The parameters n_j ($j = 1,\ 1/2$ and -1) are taken to be the same as those in Ref. [32]. [See also Table I.]

The odd-C Odderon with $\alpha_{\mathcal{O}} = 1$ has a real coupling compared to the imaginary coupling of the even C Pomeron. It reduces nuclear shadowing and produces antishadowing although it does not contribute to the free nucleon structure functions. In the following numerical estimate, we take $f_{\mathcal{O}} = 0.1$. In order to fit the large x experimental data on the parton distributions of the nucleon, we introduce different values for the parameters $\overline{\nu}^2_{-1}$ which control the off-shell dependence of the $\overline{q} - N$ amplitudes. We denote them as $\overline{\nu}^{(u)2}_{-1}$ and $\overline{\nu}^{(d)2}_{-1}$ for the u and d quarks, respectively.

We take the overall amplitude strength σ to be the same in all cases, with a value:

$$\sigma = 66 \text{ mb}. \tag{11}$$

The $I = 1$ Reggeon terms in the amplitudes play a very important role, reflecting the sea asymmetry $\overline{d} - \overline{u}$ of the nucleon in the low x region.

In principle, $I = 1$ pseudoscalar exchange should also contribute here, but the $\gamma * A \to \gamma * A$ cross section is not sensitive to its parameters, and therefore its strength cannot be fixed. Careful fits to DVCS and other processes sensitive to the $I = 1$ pseudoscalar exchanges are needed. The $I = 0$ coupling is constrained by our fit to antishadowing for electromagnetic DIS. Then we can predict antishadowing for weak DIS.

In principle, each Reggeon in the model of qN scattering amplitude should couple to the individual quarks with the appropriate isospin and charge conjugation dependence. For example, the ρ Reggeon couples as an $I = 1$, $C = -$ exchange. Although Reggeons of both $C = \pm$ appear in the quark-nucleon amplitude, in the end after multiple interactions and summing over quark and antiquark currents, the nuclear Compton amplitude has only $C = +$ exchange in the t-channel. In our model, the Reggeon term in the $q - N$ amplitude with $I = 0$ and $C = +$ is taken to represent the sum of the possible Reggeon exchanges. At leading twist only the Pomeron and Odderon which derive from gluon exchange survive in the multiple scattering. The Reggeon exchange to elastic scattering in the multiple scattering is suppressed.

In the present analysis, we also include the strange quark contribution. The antistrange quark can scatter elastically on one nucleon via Pomeron, Odderon and ϕ Reggeon exchanges. The Reggeon intercept for the ϕ trajectory is close to $\alpha_R(0) \sim 0$

since $\alpha_R(m_\phi^2) = 1$ and the Regge slope is universal. Actually, the ϕ trajectory can be parameterized as $\alpha_R(t) = 0.1 + 0.9t$ [40]. Then we can parameterize the amputated $\overline{s} - N$ and $s - N$ amplitudes as:

$$T_{\overline{s}-N} = \sigma_{\overline{s}-N}[is\beta_1^{(s)}(\tau^2) - s\beta_{\mathcal{O}}^{(s)}(\tau^2) + s^{0.1}((1+\cos 0.1\pi) - i\sin 0.1\pi)\beta_{0.1}(\tau^2)], \quad (12)$$

$$T_{s-N} = \sigma_{s-N}[is\beta_1^{(s)}(\tau^2) + s\beta_{\mathcal{O}}^{(s)}(\tau^2) + s^{0.1}((1+\cos 0.1\pi) - i\sin 0.1\pi)\beta_{0.1}(\tau^2)], \quad (13)$$

where $\sigma_{\overline{s}-N} = \sigma_{s-N} = \sigma$ and $N = p$, and n. Since the Pomeron coupling to the strange quark could be less in strength than its coupling to light quarks, $f_1^{(s)}$ should be smaller than $f_1 = 1$ for u and d quarks. We take $f_1^{(s)} = 0.1$. The value of the Reggeon coupling $f_{0.1}$ in $\beta_{0.1}(\tau^2)$ is taken as 0.2 GeV$^{0.9}$, which is the suitable mass dimension in order to have the proper mass dimension of the Reggeon terms. With the above choice of the parameters, we can produce a shape of strange quark distributions which is close to those obtained by a fit analysis [41], CTEQ-5 parametrization [42] and MRST parametrization [43].

If we use $N = p$ and n, indicating a proton and neutron target, respectively, then for an isoscalar target N_0, the amplitude $T_{\overline{q}N_0}$ per nucleon is

$$T_{\overline{q}N_0} = \frac{1}{2}(T_{\overline{q}p} + T_{\overline{q}n}). \quad (14)$$

Then we introduce

$$T_{N_0}(s,\tau^2) = T_{\overline{q}N_0}(s,\tau^2)\Delta_F^2(\tau^2), \quad (15)$$

and

$$i\Delta_F(\tau^2) \sim \frac{1}{\overline{\nu}_p^2 + \tau^2}. \quad (16)$$

Now let us turn to the scattering on a nuclear (A) target. We expect that the $\overline{q} - A$ scattering amplitude can be obtained from the $\overline{q} - N$ amplitude according to Glauber's theory as follows,

$$T_{\overline{q}A} = \sum_{k_1=0}^{Z}\sum_{k_2=0}^{N}\frac{1}{k_1+k_2}\left(\begin{array}{c} Z+N \\ k_1+k_2 \end{array}\right)\frac{1}{M}\alpha^{k_1+k_2-1}\left(T_{\overline{q}p}\right)^{k_1}\left(T_{\overline{q}n}\right)^{k_2}\theta(k_1+k_2-1) \quad (17)$$

where

$$\begin{aligned} M &= \mathrm{Min}\{\mathrm{k_1}+\mathrm{k_2},\mathrm{Z}\} - \mathrm{Max}\{\mathrm{k_1}+\mathrm{k_2}-\mathrm{N},0\}+1 \\ &= \mathrm{Min}\{\mathrm{k_1}+\mathrm{k_2},\mathrm{N}\} - \mathrm{Max}\{\mathrm{k_1}+\mathrm{k_2}-\mathrm{Z},0\}+1 \end{aligned} \quad (18)$$

and

$$\alpha = \frac{i}{4\pi p_{c.m.} s^{1/2}(R^2 + 2b)} \tag{19}$$

with

$$p_{c.m.} = \sqrt{\tau^2 + (s - M^2 - \tau^2)^2/4s}, \tag{20}$$

$$R^2 = \frac{2}{3}R_0^2, R_0 = 1.123A^{1/3}\text{fm}, \tag{21}$$

and $b = 10$ $(\text{GeV/c})^{-2}$ is used [32]. Furthermore, we introduce

$$T_A(s, \tau^2) = T_{\overline{q}A}(s, \tau^2)\Delta_F^2(\tau^2). \tag{22}$$

Similar expressions hold for T_{qA}.

The Regge contribution to the deep inelastic cross section comes from the hand-bag contribution to the forward virtual Compton amplitude $\gamma^* p \to \gamma^* p$. The Regge behavior $x^{-\alpha_R(0)}$ arises from the summation over higher Fock states. The phase of the $I = 0$ Reggeon contribution $(-i+1)$ with $\alpha_R = 1/2$ entering the virtual Compton amplitude is opposite to the positive imaginary contribution of pomeron exchange and thus tends to reduce the deep inelastic cross section on a nucleon.

As shown in Ref. [30], the multiple scattering contributions from elastic scattering from Reggeon exchange is a higher-twist contribution to the deep inelastic cross section; only gauge interactions have a FSI effect in the Bjorken limit [30]. The Pomeron and Odderon nominally have $\alpha_{\mathcal{O}} \simeq 1$, so their contributions to elastic scattering are not suppressed in the Bjorken limit, since they are derived from multiple gluon exchange. Thus the Pomeron and Odderon can act any number of times in the nucleus, but the Reggeon can act only once at leading twist. In effect the Reggeon does not have enough time to form in the FSI at small invariant separation $x^2 \sim 1/Q^2$. Thus FSIs from Reggeons in $T_{\overline{q}A}$ with $\alpha_R \sim 0.5$ should be suppressed in the Bjorken limit by a power of $1/Q$. In order to implement this we put a suppression factor R_D in the multiple scattering Reggeon terms:

$$R_D = \left(\frac{Q_0^2}{Q_0^2 + Q^2}\right)^{1/2} \tag{23}$$

for the u and d quarks. And

$$R_D = \left(\frac{Q_0^2}{Q_0^2 + Q^2}\right) \tag{24}$$

for the s quark with $Q_0^2 \simeq 1$ GeV^2, a typical hadronic scale.

When we take the limit of large Q^2, the antishadowing due to elastic Reggeon exchanges is quenched; however, the presence of the Odderon can produce antishadowing. For example, a two-step nuclear process shown in Fig. 3(b) from elastic Odderon scattering plus inelastic Reggeon scattering gives a contribution to the virtual Compton amplitude $1 \times i \times (i+1) = (-1+i)$. [The middle factor of i is due to the cut between the two steps.] The positive imaginary contribution to the two step amplitude produces an enhancement of the nuclear cross section relative to the nucleon cross section in the regime $x \sim 0.1$ where the Reggeon contribution to deep inelastic scattering is important. This is a key feature of our model. Note that the two-step process of Odderon plus Pomeron produces only a real contribution to the virtual Compton amplitude. The Pomeron-Pomeron and Pomeron-Reggeon two-step contributions reduce the one-step Pomeron plus Reggeon contributions, respectively, and thus only produce nuclear shadowing.

We can also consider the two-step $[PiR_\pi]$ contribution to $Im\ T_{\gamma^* A \to \gamma^* A}$, which involves the imaginary part $Im\ R_\pi$ of the (nonforward) pion Reggeon exchange amplitude. The pion pole term alone is real so we consider the pion Regge trajectory—the Reggeized version of pion exchange. When we take its absorptive part, we look at the cut through a $q\overline{q}$ ladder exchanged on the second nucleon. Since the Reggeized pion exchange has $I = 1$ and the pomeron is $I = 0$, the two-step $[PiR_\pi]$ contribution does not contribute to $Im\ T_{\gamma^* A \to \gamma^* A}$ if the target is $I = 0$ Thus there is no antishadowing contribution from $[PiR_\pi]$ to the deuteron structure function. However, there are other pseudoscalar exchanges possible, such as the η Reggeon.

It is interesting to analyze the situation form the point of view of angular momentum. The question is whether the two step process $[PiR_\pi]$ require orbital angular momentum in the ground state nuclear wavefunction. Consider the $[PiR_\pi]$ contribution to the forward virtual Compton amplitude $Im\ T_{\gamma^* A \to \gamma^* A}$. The pomeron exchange on the first nucleon gives a transverse momentum kick $\vec{k}_\perp$. The pion Reggeon exchange on the second nucleon gives a balancing opposite kick $-\vec{k}_\perp$ so that we can have a forward nuclear amplitude. The pseudoscalar exchange on the second nucleon is a $\Delta L = 1$ transition. That is why the amplitude requires nonzero $k_\perp$. Thus we

are actually looking at the overlap of nuclear Fock components of the nucleus with $\Delta L = 1$. This is the same admixture which in the spin-1/2 case which gives a nuclear magnetic anomalous moment.

The unpolarized quark distribution functions in an isoscalar target (N_0) and nucleus target (A) are, respectively,

$$xq^{N_0}(x) = \frac{2}{(2\pi)^3}\frac{Cx^2}{1-x}\int dsd^2\mathbf{k}_\perp \mathrm{ImT_{N_0}(s,\mu^2)}, \tag{25}$$

$$xq^{A}(x) = \frac{2}{(2\pi)^3}\frac{Cx^2}{1-x}\int dsd^2\mathbf{k}_\perp \mathrm{ImT_{A}(s,\mu^2)}, \tag{26}$$

$$\mu^2 = -\tau^2. \tag{27}$$

The constant C is related to the parton wave function renormalization constant.

With the obtained quark distributions $xq^{N_0(A)}(x)$ for an isoscalar target N_0 or a nucleus target A, we can calculate the structure functions for various current exchanges.

(1) The photon exchange case

$$F_1^{\gamma N_0(A)} = \frac{1}{2}\Bigg\{\frac{4}{9}\left[u(x)^{N_0(A)}+\overline{u}^{N_0(A)}\right]+\frac{1}{9}\Big[d(x)^{N_0(A)}+\overline{d}^{N_0(A)} + s(x)^{N_0(A)}+\overline{s}^{N_0(A)}\Big]\Bigg\}, \tag{28}$$

$$F_2^{\gamma N_0(A)} = 2xF_1^{\gamma N_0(A)}. \tag{29}$$

(2) The neutral current exchange case

The structure functions of the NC reaction are

$$F_1^{ZN_0(A)} = \frac{1}{2}\Bigg\{\left[(g_V^u)^2+(g_A^u)^2\right](u^{N_0(A)}(x)+\overline{u}^{N_0(A)}(x)) + [(g_V^d)^2+(g_A^d)^2]\left(d^{N_0(A)}(x)+\overline{d}^{N_0(A)}(x)+s^{N_0(A)}(x)+\overline{s}^{N_0(A)}(x)\right)\Bigg\}, \tag{30}$$

$$F_2^{ZN_0(A)} = 2xF_1^{ZN_0(A)}, \tag{31}$$

$$F_3^{ZN_0(A)} = 2\Big[g_V^u g_A^u(u^{N_0(A)}(x)-\overline{u}^{N_0(A)}(x)) + g_V^d g_A^d(d^{N_0(A)}(x)-\overline{d}^{N_0(A)}(x)+s^{N_0(A)}(x)-\overline{s}^{N_0(A)}(x))\Big]. \tag{32}$$

In the SM the vector and axial-vector quark couplings are given by

$$g_V^u = \frac{1}{2} - \frac{4}{3}\sin^2\theta_W, \quad g_V^d = -\frac{1}{2} + \frac{2}{3}\sin^2\theta_W, \quad g_A^u = \frac{1}{2}, \quad g_A^d = -\frac{1}{2},$$

where $\sin^2\theta_W$ is the weak-mixing angle.

(3) The charged current exchange case

The structure function of the CC reaction is given by

$$\begin{aligned} F_1^{W^+N_0(A)} &= \overline{u}^{N_0(A)}(x)(|V_{ud}|^2 + |V_{us}|^2) + \overline{u}^{N_0(A)}(\xi_b)|V_{ub}|^2\theta(x_b - x) \\ &+ d^{N_0(A)}(x)|V_{ud}|^2 + d^{N_0(A)}(\xi_c)|V_{cd}|^2\theta(x_c - x) \\ &+ s^{N_0(A)}(x)|V_{us}|^2 + s^{N_0(A)}(\xi_c)|V_{cs}|^2\theta(x_c - x), \end{aligned} \tag{33}$$

here V_{ij} are the Cabibbo-Kobayashi-Maskawa mixing matrix elements. The variable

$$\xi_k = \begin{cases} x\left(1 + \frac{m_k^2}{Q^2}\right), & (k = c, b), \\ x, & (k = u, d, s), \end{cases}$$

and the step functions $\theta(x_c - x), \theta(x_b - x)$ take into account rescaling due to heavy quark production thresholds.

The structure functions $F_2^{W^+N_0(A)}$ and $F_3^{W^+N_0(A)}$ are obtained from (33) by the replacement of the quark distribution functions $q(x, Q^2)$ indicated in the curly brackets:

$$\begin{aligned} F_2^{W^+N_0(A)}(x, Q^2) &= F_1^{W^+N_0(A)}(x, Q^2)\{q^{N_0(A)}(x, Q^2) \to 2xq^{N_0(A)}(x, Q^2), \\ &\quad q^{N_0(A)}(\xi_k, Q^2) \to 2\xi_k q^{N_0(A)}(\xi_k, Q^2)\}, \end{aligned} \tag{34}$$

$$F_3^{W^+N_0(A)}(x, Q^2) = 2\ F_1^{W^+N_0(A)}(x, Q^2)\{\overline{q}^{N_0(A)}(x, Q^2) \to -\overline{q}^{N_0(A)}(x, Q^2)\}. \tag{35}$$

There are similar formulas for the W^--current exchange reaction.

2.2 The values of the parameters

In the last section we presented the formulas involved in our formalism. We shall take the value for most of the parameters to be the same as those in Ref. [32]. The values of other parameters are chosen in order to fit the experimental data [44, 45, 46] on

$F_2^{N_0}$,$(F_2^p - F_2^n)$, F_2^n/F_2^p; they are then checked against the known nuclear shadowing and antishadowing effects [47, 48]. A summary of the set of parameters is given in Table 1.

Table 1: Parameters in our numerical calculation

$\overline{\nu}_1^2$	0.2 GeV^2	f_1, f_1^s	1.0, 0.5
$\overline{\nu}_{1/2}^2$	0.2 GeV^2	$f_{1/2}^{0+}$, $f_{1/2}^{0-}$, $f_{1/2}^{1+}$, $f_{1/2}^{1-}$	0.30,0.3,0.1,0.3 GeV
$\overline{\nu}_{-1}^{(u)2}$, $\overline{\nu}_{-1}^{(d)2}$	1.3, 0.65 GeV^2	f_{-1}	0.45 GeV^4
$\overline{\nu}_{\mathcal{O}}^2$	0.30 GeV^2	$f_{\mathcal{O}}$	0.10
$\overline{\nu}_p^2$	1.0 GeV^2	b	10 (GeV/c)$^{-2}$
σ	66 mb	n_{-1}	2
$f_{\rm pseudo}$	1.35 GeV	n_1, $n_{1/2}$, n_0	4

With the above parameters, the average nucleon structure function

$$F_2 = F_2^{N_0} = \frac{F_2^p + F_2^n}{2} \tag{36}$$

for the photon exchange case are shown as a solid curve in Fig. 4. The valence and sea contributions to F_2 are also presented as dashed and dotted curves in Fig. 4. F_2 is close to the SLAC and NMC [46] experimental data. We also show our results of the difference $F_2^p - F_2^n$ and the ratio F_2^n/F_2^p of the nucleon structure functions in Fig. 5 and Fig. 6, respectively. In the coming subsection we will show the nuclear effects on the structure functions and in the next section estimate the nuclear shadowing and antishadowing effects on the extraction of $\sin^2\theta_W$.

2.3 Nuclear shadowing and antishadowing effects

We introduce the ratio

$$R = F_2^A/F_2^{N_0} \tag{37}$$

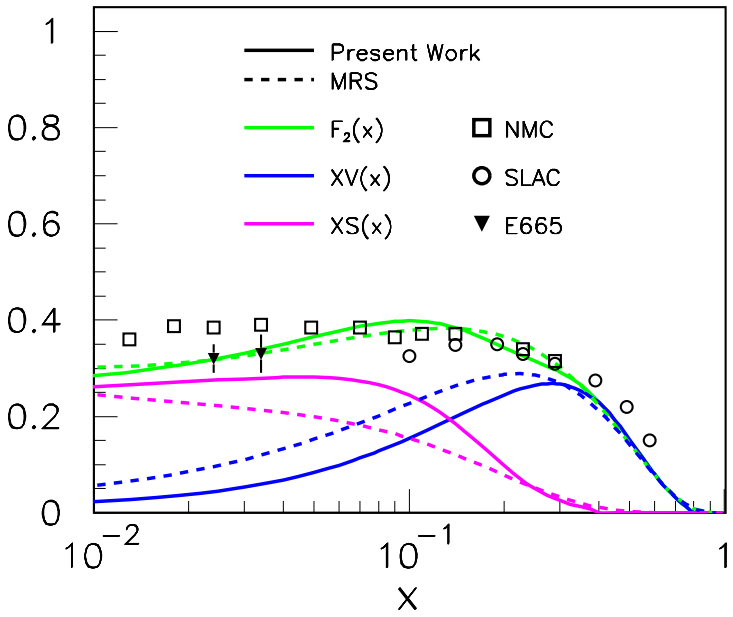

Figure 4: The calculated nucleon structure function F_2 (biggest solid curve), and valence (next solid curve at large x values) and sea (smallest solid curve at large x values) contributions to F_2, and the corresponding result of the MRST parametrization [43] (dashed curves), at $Q^2 = 1$ GeV^2. The experimental data are taken from Ref. [46].

to indicate the nuclear electromagnetic shadowing and antishadowing effect. We will focus on the nucleus ^{56}Fe since an iron target was used in the NuTeV experiment and test the nuclear effect in the $x > 0.01$ region since 97% of the NuTeV data is from $0.01 < x < 0.75$ [50]. In Figs. 7–8, we show the quark q and anti-quark $\overline{q}$ contributions to the ratio of the structure functions. In order to stress the individual contribution of quarks, the numerator of the ratio $F_2^A/F_2^{N_0}$ shown in these two figures is obtained from the denominator by a replacement $q^{N_0}(\overline{q}^{N_0})$ into $q^A(\overline{q}^A)$ for only the considered quark (anti-quark). Because the strange quark distribution is much smaller than u and d quark distributions, the strange quark contribution to the ratio is very close to 1 although s^A/s^{N_0} may significantly deviate from 1.

In Fig. 9, we give our prediction of the nuclear shadowing and antishadowing effects (the sum of all quark and antiquark contributions to the ratio R) for nuclei ^{56}Fe and ^{40}Ca. From Fig. 9, we find that our model can explain well the experimental

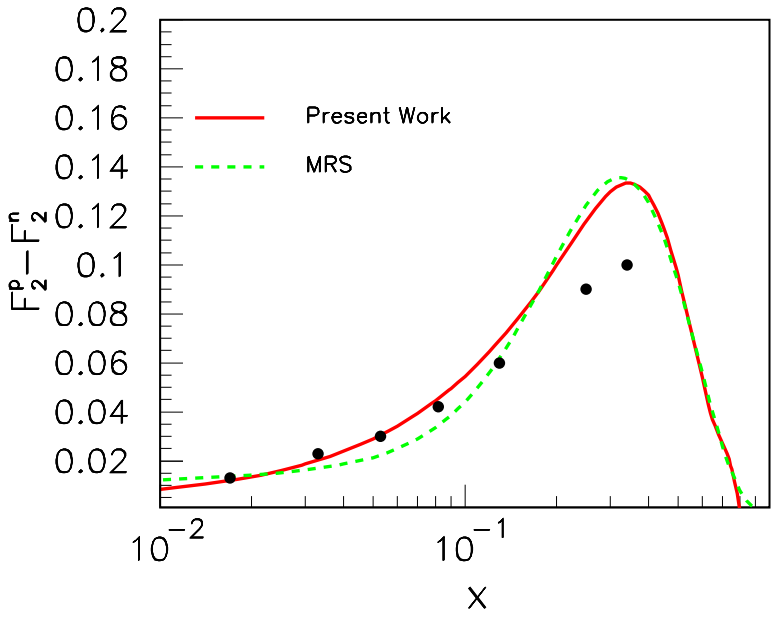

Figure 5: The calculated difference $F_2^p - F_2^n$ of the nucleon structure functions (solid curve), and the corresponding result of the MRST parametrization [43](dashed curve), at $Q^2 = 1$ GeV^2. The experimental data are taken from Ref. [45].

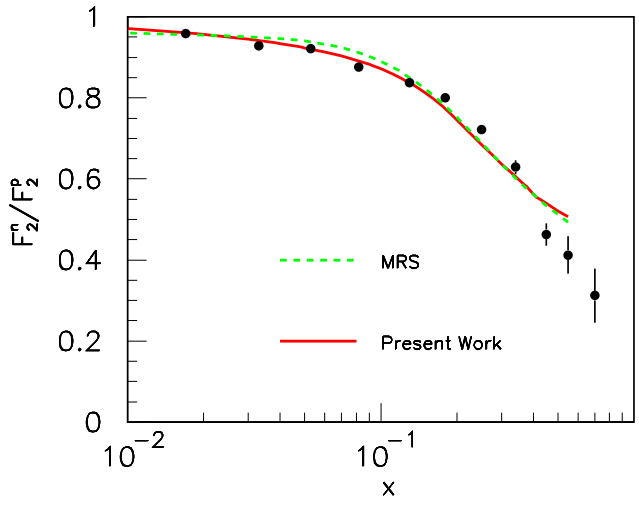

Figure 6: The calculated ratio F_2^n/F_2^p of the nucleon structure functions (solid curve), and the corresponding result of the MRST parametrization [43] at energy scale 1 GeV (dashed curve). The experimental data are taken from Ref. [45].

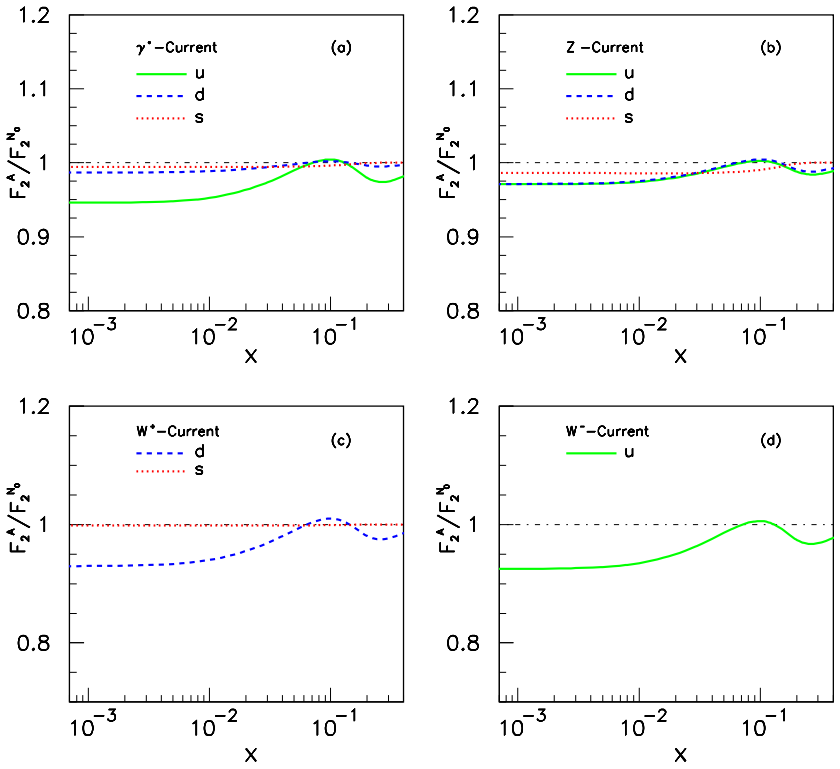

Figure 7: The quark contributions to the ratios of structure functions at $Q^2 = 1$ GeV^2. The solid, dashed and dotted curves correspond to the u, d and s quark contributions, respectively. This corresponds in our model to the nuclear dependence of the $\sigma(\overline{u}-A)$, $\sigma(\overline{d}-A)$, $\sigma(\overline{s}-A)$ cross sections, respectively. In order to stress the individual contribution of quarks, the numerator of the ratio $F_2^A/F_2^{N_0}$ shown in these two figures is obtained from the denominator by a replacement q^{N_0} into q^A for only the considered quark. As a result, the effect of antishadowing appears diminished.

data on the nuclear shadowing and antishadowing effect in DIS for electromagnetic currents.

We can further check the our model by predicting the ratio of F_2 structure functions F_{2A}[neutrino]/(18/5)F_{2A}[muon], which has been measured by the NuTev collaboration [49]. The results are shown in Fig.10, and they agree very well with the experimental data, in a calculation with no further free parameters. Notice that the data for the ratio tends to go below 1 for $x > 0.4$, which is also what we find. In this case we have taken $Q^2 = 20$ GeV^2, which is the average value of the NuTeV experiment.

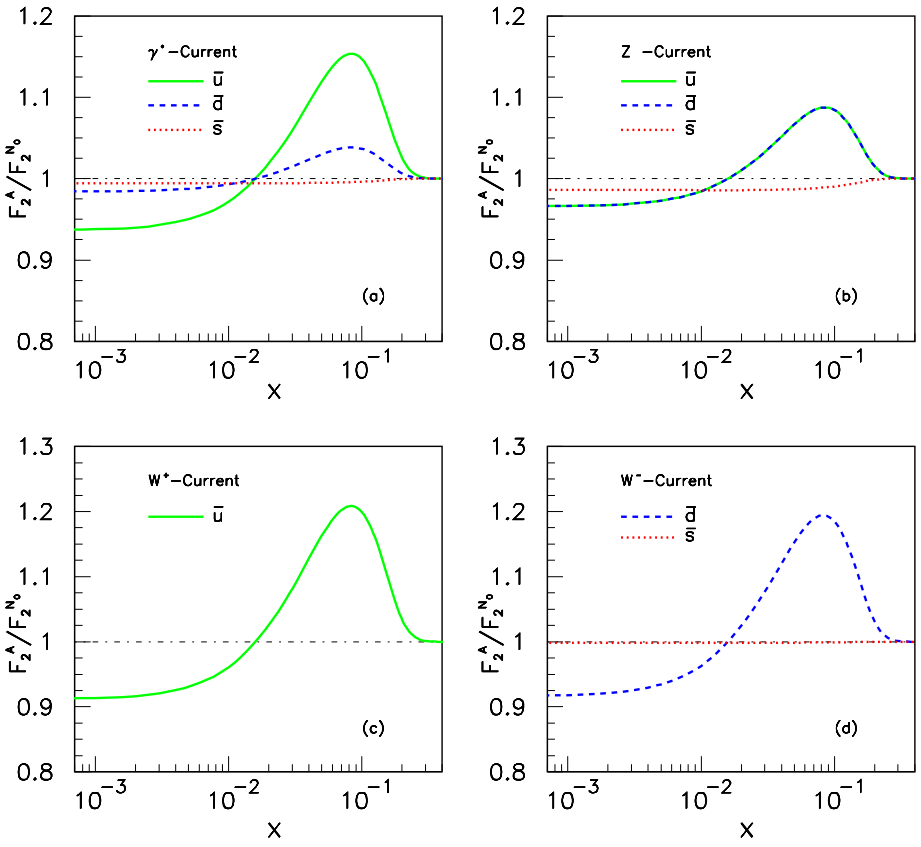

Figure 8: The anti-quark contributions to ratios of the structure functions at $Q^2 = 1$ GeV^2. The solid, dashed and dotted curves correspond to $\overline{u}$, $\overline{d}$ and $\overline{s}$ quark contributions, respectively. This corresponds in our model to the nuclear dependence of the $\sigma(u-A)$, $\sigma(d-A)$, $\sigma(s-A)$ cross sections, respectively. In order to stress the individual contribution of quarks, the numerator of the ratio $F_2^A/F_2^{N_0}$ shown in these two figures is obtained from the denominator by a replacement $\overline{q}^{N_0}$ into $\overline{q}^A$ for only the considered anti-quark.

We emphasize that the nuclear shadowing and antishadowing of the different currents are not universal since they depend on the different quark species. We still have factorization in the sense that we will have the same shadowing quark by quark in nuclear Drell-Yan processes.

In the case of weak currents, the shadowing/antishadowing effects are strongly influenced by the behavior of the structure function F_3, which is not present in the electromagnetic case. We will present in the next section cross section ratios (nucleus/nucleon) to illustrate the shadowing/antishadowing effects in weak current

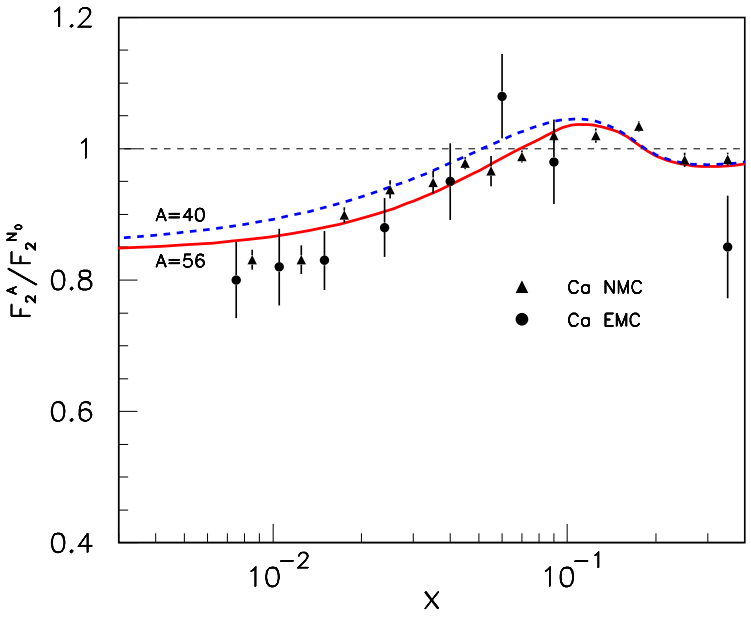

Figure 9: The nuclear shadowing and antishadowing effects at $\langle Q^2 \rangle = 1$ GeV^2. The experimental data are taken from Refs. [47, 48].

interactions.

3 Nuclear effects on extraction of $\sin^2\theta_W$

The observables measured in neutrino DIS experiments are the ratios of neutral current (NC) to charged current (CC) current events; these are related via Monte Carlo simulations to $\sin^2\theta_W$. In order to examine the possible impact of nuclear shadowing and antishadowing corrections on the extraction of $\sin^2\theta_W$, one is usually interested in the following ratios

$$R_A^\nu = \frac{\sigma(\nu_\mu + A \to \nu_\mu + X)}{\sigma(\nu_\mu + A \to \mu^- + X)}, \tag{38}$$

$$R_A^{\overline{\nu}} = \frac{\sigma(\overline{\nu}_\mu + A \to \overline{\nu}_\mu + X)}{\sigma(\overline{\nu}_\mu + A \to \mu^+ + X)} \tag{39}$$

of NC to CC neutrino (anti-neutrino) cross sections for a nuclear target A. As is well known, if nuclear effects are neglected for an isoscalar target, one can extract the

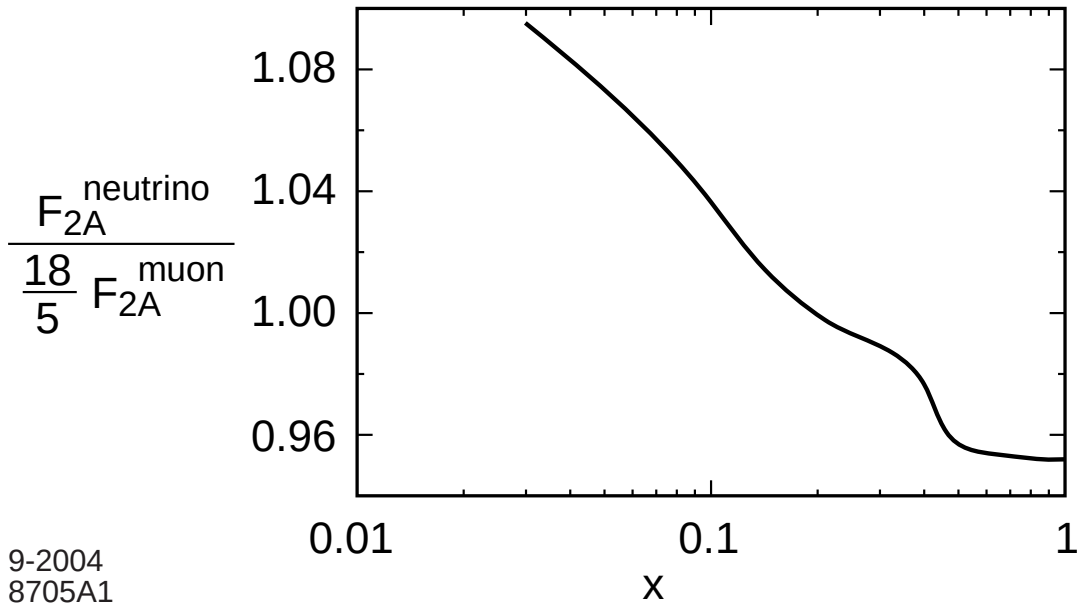

Figure 10: Our prediction for the ratio of F_2 structure functions F_{2A}[neutrino]/(18/5)F_{2A}[muon], measured in Ref. [49], at $Q^2 = 20$ GeV^2.

weak-mixing angle by using the Llewellyn-Smith relation [51]:

$$R_N^{\nu[\overline{\nu}]} = \frac{\sigma(\nu_\mu[\overline{\nu}_\mu] + N \to \nu_\mu[\overline{\nu}_\mu] + X)}{\sigma(\nu_\mu[\overline{\nu}_\mu] + N \to \mu^-[\mu^+] + X)} = \rho_0^2 \left(\frac{1}{2} - \sin^2\theta_W + \frac{5}{9}\sin^4\theta_W(1 + r^{[-1]})\right), \quad (40)$$

written in terms of NC and CC (anti-)neutrino-nucleon cross sections. Here,

$$\rho_0 = \frac{M_W^2}{\cos^2\theta_W M_Z^2}, \qquad r = \frac{\sigma(\overline{\nu}_\mu + N \to \mu^+ + X)}{\sigma(\nu_\mu + N \to \mu^- + X)} \sim \frac{1}{2}. \quad (41)$$

However, actual targets such as the iron target of the NuTeV experiment are not always isoscalar, having a significant neutron excess. In addition, as we have stressed here, nuclear effects due to multi-scattering could be very important. These nuclear effects should also modify the CC and NC structure functions, and therefore a detailed study of these effects on the extraction of the weak-mixing angle is essential. In order to reduce the uncertainties related to sea quarks, Paschos and Wolfenstein [52] showed that one can extract $\sin^2\theta_W$ from the relationship

$$R_N^- = \frac{\sigma(\nu_\mu + N \to \nu_\mu + X) - \sigma(\overline{\nu}_\mu + N \to \overline{\nu}_\mu + X)}{\sigma(\nu_\mu + N \to \mu^- + X) - \sigma(\overline{\nu}_\mu + N \to \mu^+ + X)} = \rho_0^2 \left(\frac{1}{2} - \sin^2\theta_W\right). \quad (42)$$

Inspired by the above relation, we will examine nuclear effects on $\sin^2\theta_W$ by the following observable for the scattering off a nuclear target A,

$$R_A^- = \frac{\sigma(\nu_\mu + A \to \nu_\mu + X) - \sigma(\overline{\nu}_\mu + A \to \overline{\nu}_\mu + X)}{\sigma(\nu_\mu + A \to \mu^- + X) - \sigma(\overline{\nu}_\mu + A \to \mu^+ + X)}. \tag{43}$$

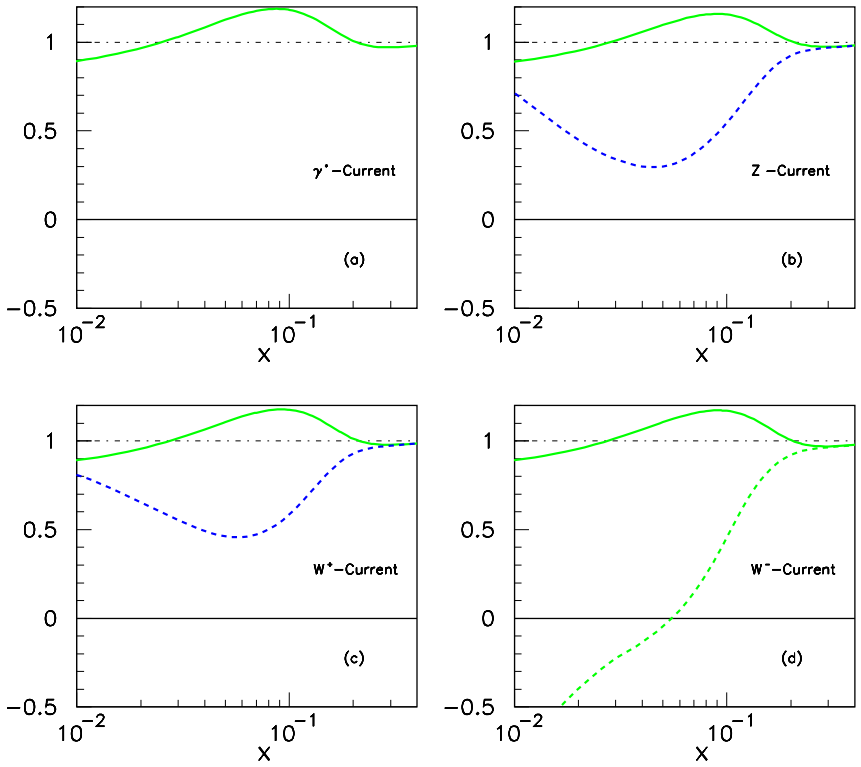

Figure 11: Ratios $F_2^A/F_2^{N^0}$ (solid curves) and $F_3^A/F_3^{N^0}$ (dashed curves) for various current exchange interactions, at $Q^2 = 1$ GeV^2.

In the previous section, we have shown in Fig. 9 the nuclear effect on the electromagnetic structure functions. Here we can also look the nuclear effect on the cross sections in CC and NC neutrino-nucleus DIS. In Fig. 11, we show ratios $F_2^A/F_2^{N^0}$ (solid curves) and $F_3^A/F_3^{N^0}$ (dashed curves) for various current exchange interactions. The fact that the $F_3^A/F_3^{N^0}$ ratio for the W^--current becomes negative and divergent for small x comes from the behavior of $F_3^{N^0}$, which in our model vanishes for $x \sim 0.01$. In addition, we are interested in the following ratios

$$R_Z^\nu(x) = \frac{d\sigma(\nu_\mu + A \to \nu_\mu + X)/dx}{d\sigma(\nu_\mu + N \to \nu_\mu + X)/dx}, \tag{44}$$

$$R_Z^{\overline{\nu}}(x) = \frac{d\sigma(\overline{\nu}_\mu + A \to \overline{\nu}_\mu + X)/dx}{d\sigma(\overline{\nu}_\mu + N \to \overline{\nu}_\mu + X)/dx}, \tag{45}$$

$$R_{W^+}^{\nu}(x) = \frac{d\sigma(\nu_\mu + A \to \mu^- + X)/dx}{d\sigma(\nu_\mu + N \to \mu^- + X)/dx}, \tag{46}$$

$$R_{W^-}^{\overline{\nu}}(x) = \frac{d\sigma(\overline{\nu}_\mu + A \to \mu^+ + X)/dx}{d\sigma(\overline{\nu}_\mu + N \to \mu^+ + X)/dx}. \tag{47}$$

The above ratios are closely related to the nuclear effects in the ratio,

$$R_{A/N}^- = R_A^-/R_N^- \tag{48}$$

which are later used to extract the nuclear effect on the weak-mixing angle. In Fig. 12, we show the ratios of Eqs. (44)–(47). From Figs. 9–12, one finds that the nuclear effect for charged and neutral currents is substantially different from that for the electromagnetic nuclear structure functions. There is a strong antishadowing effect in $R_Z^{\overline{\nu}}$ and $R_{W^-}^{\overline{\nu}}$, but there is a small one in R_Z^{ν} and $R_{W^+}^{\nu}$. Moreover, for neutrinos the NC and CC shadowing/antishadowing effects are the same, but for antineutrinos they are substantially different. As a result, in the neutrino case the Llewellyn-Smith relation can be used in order to extract the weak mixing angle, but it cannot be used for this purpose in the case of antineutrino deep inelastic scattering in nuclei.

If the nuclear target had zero isospin, and there was no contribution from s or $\overline{s}$ quarks, then there would be no nuclear correction to the Llewellyn Smith relation. However, when one includes the strange quark currents, the situation is different. The neutral current interactions of the antineutrino on the $\overline{s}$ are shadowed rather than antishadowed (see Fig. 11) in the region $x \sim 0.1$, which reduces the total antishadowing effect. The charged current interactions of the antineutrino still experience strong antishadowing from the $\overline{d}$. In contrast, neutrino interactions are relatively insensitive to the strange quark current since they are dominated by interactions on the valence quarks, not the anti-quarks. Even when one includes the strange quarks, antineutrino NC and CC interactions experience more antishadowing than neutrinos (see Fig. 12).

An alternative way of assessing the nuclear corrections is through a modified Paschos-Wolfenstein ratio $R_A^-(x)/R_N^-(x)$, in which instead of the total cross section we consider the corresponding differential cross sections, as shown in Fig. 13. In

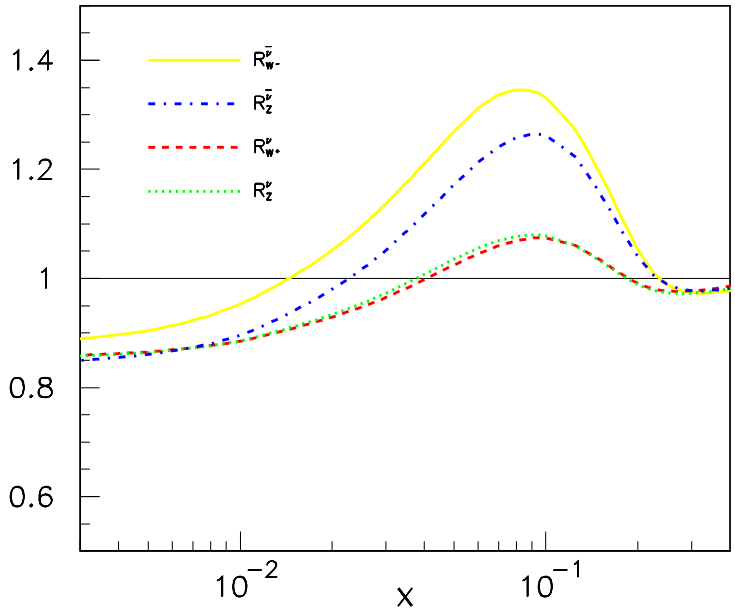

Figure 12: The nuclear effect on the cross sections of CC and NC neutrino-nucleus DIS, at $Q^2 = 1$ GeV^2. The dotted and dashed curves almost overlap.

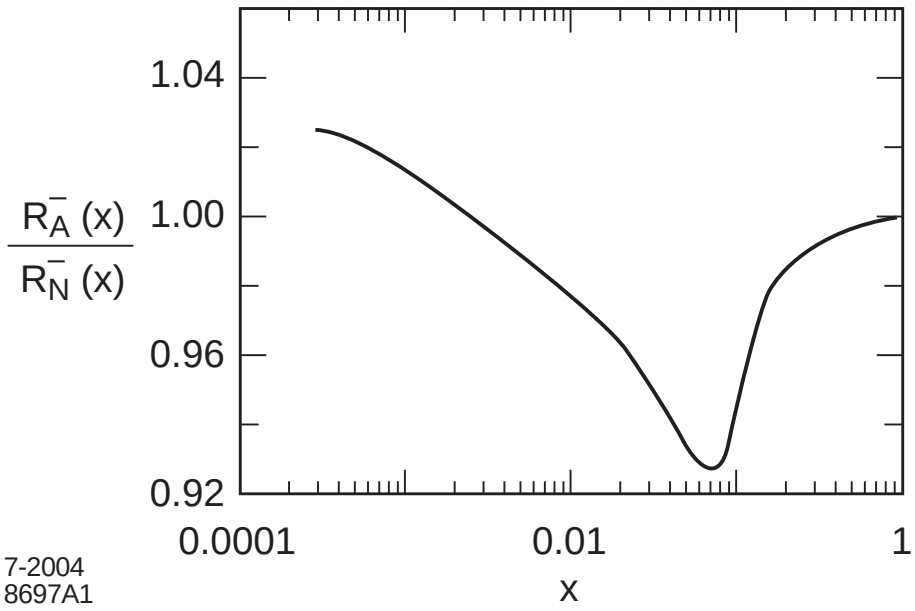

Figure 13: The nuclear effect on the Paschos-Wolfenstein ratio of differential cross sections $R_A^-(x)/R_N^-(x)$, at $Q^2 = 20$ GeV^2.

this case we have taken $Q^2 = 20$ GeV^2, which is the average value of the NuTeV experiment.

In our numerical analysis we studied the influence of nuclear effects on the extraction of $\sin^2\theta_W$ from the observable R_A^-, taking into account some kinematical cut-offs specific to the NuTeV experiment.

The differential cross sections for CC and NC (anti-)neutrino-nucleus deep inelastic scattering are given by [53]

$$\begin{aligned}\frac{d^2\sigma_{CC}^{\nu,\overline{\nu}\ (A)}}{dxdy} &= \frac{G_F^2}{\pi}\ m_N\ E_{\nu,\overline{\nu}}\Big\{xy^2F_1^{W^\pm(A)}(x,Q^2)+ \\ &+ \left(1-y-\frac{xym_N}{2\ E_{\nu,\overline{\nu}}}\right)F_2^{W^\pm(A)}(x,Q^2)\pm\left(y-\frac{y^2}{2}\right)xF_3^{W^\pm(A)}(x,Q^2)\Big\},\end{aligned} \tag{49}$$

for the CC reaction, and

$$\begin{aligned}\frac{d^2\sigma_{NC}^{\nu,\overline{\nu}\ (A)}}{dxdy} &= \frac{G_F^2}{\pi}\ m_N\ E_{\nu,\overline{\nu}}\Big\{xy^2F_1^{Z(A)}(x,Q^2)+ \\ &+ \left(1-y-\frac{xym_N}{2\ E_{\nu,\overline{\nu}}}\right)F_2^{Z(A)}(x,Q^2)\pm\left(y-\frac{y^2}{2}\right)xF_3^{Z(A)}(x,Q^2)\Big\},\end{aligned} \tag{50}$$

for the NC reaction.

In the event selection, the NuTeV Collaboration applied the cut off

$$20\ \ \text{GeV} \leq \text{E}_{\text{cal}} \leq 180\ \ \text{GeV}, \tag{51}$$

for a visible energy deposit to the calorimeter E_{cal}. The lower limit ensures full efficiency of the trigger, allows for an accurate vertex determination and reduces cosmic ray background.

Therefore we will calculate the observables $R_A^{\nu(\overline{\nu})}$ and R_A^- imposing the same cut off on the energy E_h of the final hadronic state X assuming $E_h = E_{\text{cal}}$. Since $E_h \approx \nu$, we can write the kinematical variables averaged over the (anti-)neutrino flux as

$$x = \frac{Q^2}{2M_N E_{\text{cal}}} \leq 1, \qquad y = \frac{E_{\text{cal}}}{\langle E_{\nu(\overline{\nu})}\rangle} \leq 1. \tag{52}$$

For the average energies of the neutrino and antineutrino beams we take the values $\langle E_\nu\rangle = 120$ GeV and $\langle E_{\overline{\nu}}\rangle = 112$ GeV, as in the NuTeV experiment [54].

We will assume a modified version of the Paschos-Wolfenstein relation:

$$\begin{aligned} R_N^-(\sin^2\theta_W) &= \rho_0^2(1+\varepsilon)\left(\frac{1}{2}-\sin^2\theta_W\right) \\ &= \rho^2\left(\frac{1}{2}-\sin^2\theta_W\right), \end{aligned} \tag{53}$$

where, $\rho^2 = \rho_0^2(1+\varepsilon)$ with a modified factor $(1+\varepsilon)$ due to strange quark, isospin breaking, threshold corrections for heavy quarks production, and so on. We further assume that the Paschos-Wolfenstein relation can be applied to the scattering on a nuclear target A,

$$R_A^-(\sin^2\theta_W) = \rho^2\left(\frac{1}{2}-(\sin^2\theta_W+\Delta\sin^2\theta_W)\right). \tag{54}$$

with a correction $\Delta\sin^2\theta_W$ to the weak-mixing angle. In Fig. 14(a), we show the $\sin^2\theta_W$ dependence in the ratio $R_{A/N}^-$. We estimate $\Delta\sin^2\theta_W$ in the following way. First, we use the cross sections to calculate the Paschos-Wolfenstein ratios $R_A^-(\sin^2\theta_W)$ and $R_N^-(\sin^2\theta_W)$ with various values of $\sin^2\theta_W$. Second, we extract ρ^2 by means of Eq. (53). In principle, ρ^2 should be different for various values of $\sin^2\theta_W$. We find a weak dependence of ρ^2 on $\sin^2\theta_W$ and $\rho^2 \simeq 1.04$. Finally, we use the obtained ρ^2 to extract the shadowing/antishadowing effect on the weak-mixing angle $\Delta\sin^2\theta_W$ from Eq. (54). The results are given in Fig. 14(b).

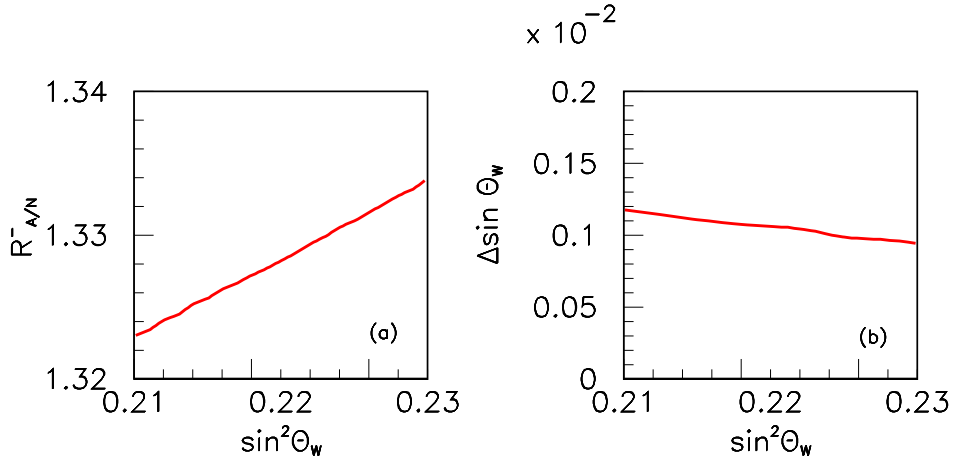

Figure 14: (a) The $\sin^2\theta_W$ dependence in $R_{A/N}^-$; (b) The nuclear shadowing/antishadowing corrections to the $\sin^2\theta_W$.

We have performed a numerical calculation at the average $\langle Q^2 \rangle = 20$ GeV^2 of the NuTeV experiment and have found that the modification to the weak-mixing angle is approximately $\delta \sin^2 \theta_W = 0.001$. The value of $\sin^2 \theta_W$ determined from the NuTeV experiment, without including nuclear shadowing/antishadowing due to multiple scattering, is in absolute value 0.005 larger than the best value obtain from other experiments. The model used here to compute nuclear shadowing/antishadowing effect would reduce the discrepancy between the neutrino and electromagnetic measurements of $\sin^2 \theta_W$ by about 20%. Together with the charge symmetry violation contributions to the neutrino reactions [55], about half of the difference between the standard model and the NuTeV result can be accounted for. We also note that the antishadowing effects we predict are most important in the antineutrino data, which is less sensitive to $\sin^2 \theta_W$.

4 Conclusions

We have investigated nuclear shadowing and antishadowing effects arising from the multiple scattering of quarks and anti-quarks in the nucleus. The effective quark-nucleon scattering amplitude includes Pomeron and Odderon contributions from multi-gluon exchange as well as Reggeon quark-exchange contributions. The model is constrained by measurements of the nuclear structure functions in deep inelastic electron and muon scattering as well as the Regge behavior of the non-singlet structure functions. We have also noted the possibility of obtaining an antishadowing contribution from one-gluon exchange $\times$ Reggeon exchange, assuming the existence of hidden-color components in the nuclear wavefunction. We have shown that the coherence of these multiscattering nuclear processes leads to shadowing and antishadowing of the electromagnetic nuclear structure functions in agreement with measurements. The momentum sum rule is not satisfied in a nuclear target by balancing the shadowing and antishadowing of the leading-twist nuclear quark distributions; however the momentum sum rule can still be satisfied if there is a compensating change in the nuclear gluon distribution.

Our analysis leads to substantially different nuclear antishadowing for charged

and neutral current reactions; in fact, the neutrino and antineutrino DIS cross sections are each modified in different ways due to the various allowed Regge exchanges. The non-universality of nuclear effects will modify the extraction of the weak-mixing angle $\sin^2\theta_W$, particularly because of the strong nuclear effects for the F_3 structure function. The shadowing and antishadowing of the strange quark structure function in the nucleus can also be considerably different than that of the light quarks. We thus find that part of the anomalous NuTeV result for $\sin^2\theta_W$ could be due to the nonuniversality of nuclear antishadowing for charged and neutral currents. Our picture also implies non-universality for the nuclear modifications of spin-dependent structure functions.

We have found in our analysis that the antishadowing of nuclear structure functions depends in detail on quark flavor. Careful measurements of the nuclear dependence of charged, neutral, and electromagnetic DIS processes are thus needed to establish the distinctive phenomenology of shadowing and antishadowing and to make the NuTeV results definitive. It is also important to map out the shadowing and antishadowing of each quark component of the nuclear structure functions to illuminate the underlying QCD mechanisms. Such studies can be carried out in semi-inclusive deep inelastic scattering for the electromagnetic current at Hermes and at Jefferson Laboratory by tagging the flavor of the current quark or by using pion and kaon-induced Drell-Yan reactions. A new determination of $\sin^2\theta_W$ is also expected from the neutrino scattering experiment NOMAD at CERN [57]. A systematic program of measurements of the nuclear effects in charged and neutral current reactions could also be carried out in high energy electron-nucleus colliders such as HERA and eRHIC, or by using high intensity neutrino beams [58].

Appendix: A non-abelian source for antishadowing

We can identify a further antishadowing contribution specific to the non-abelian theory. Consider once again Fig. 2 for $\gamma^* A \to \gamma^* A$, but replace the two exchanged gluons with just a single gluon (see Fig. 15). For simplicity we display the case of a deuteron target. In Fig. 4(a) the exchanged gluon attaches to the struck u quark valence constituent of the proton at the top of the diagram changing its color.

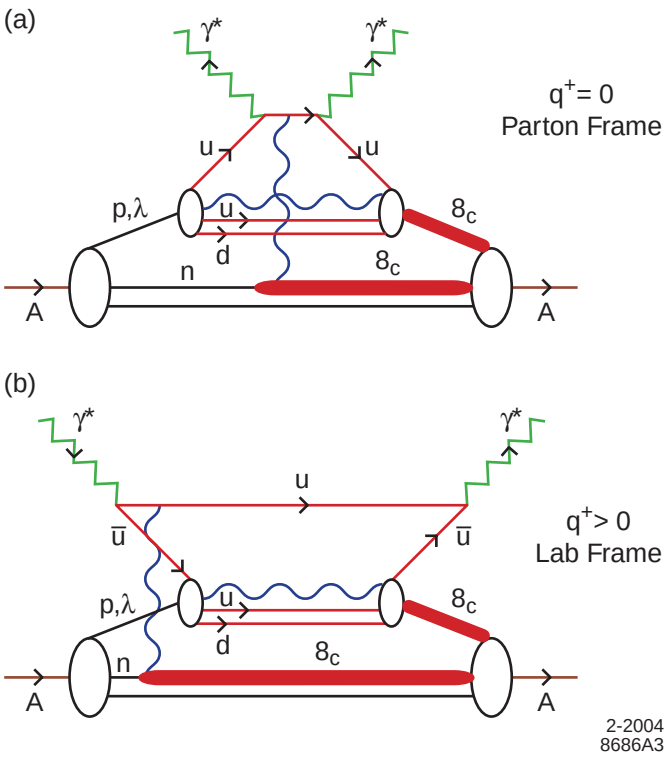

Figure 15: Representation of leading-twist QCD "hidden color" contributions to the nuclear structure function from the absorptive part of the forward virtual Compton amplitude $Im\, T(\gamma^* A \to \gamma^* A)$. (a) Illustration of a two-step contribution in the $q^+ = 0, q_\perp^2 = Q^2$ parton model frame—deep inelastic lepton scattering on a valence quark of a target proton followed by the final-state single-gluon interaction of the outgoing quark on a target neutron. The proton and neutron are both color excited to color-octet states. The amplitude requires the presence of hidden-color components in the nuclear wavefunction. (b) Illustration of the physics of the two-step process shown in (a), but in the laboratory frame where $q^+ > 0$. The $u\overline{u}$ fluctuation of the virtual photon first scatters via a single gluon exchange on a neutron; this is then followed by the annihilation of the $\overline{u}$ quark on a proton. The proton and neutron are both color excited to color-octet states. The amplitude requires the presence of hidden-color components in the nuclear wavefunction. The two-step amplitude can interfere constructively with the Regge-behaved single-step annihilation amplitude on the proton alone, thus producing antishadowing. Similar processes occur in the case of the weak currents.

This also changes the scattered proton p' to a color octet. The exchanged gluon also transforms the spectator neutron into a color octet. Thus if the deuteron wavefunction contains hidden color $|8_C 8_C\rangle$ components, this process interferes with the one step diagram with no final state interactions.

The deuteron certainly has hidden-color components—one only has to exchange a gluon between the nucleons in the deuteron LFWF [59]. The large magnitude of the deuteron form factor also demands hidden color components ([56]). The calculation of the one-gluon exchange effects is very similar to our Odderon analysis. The one-gluon exchange amplitude behaves as s^1 and a nearly real phase. Like the Odderon, it has $C = -$ and couples with opposite sign to the q and $\overline{q}$. A complication is how to understand the Reggeon exchange amplitude on the proton since the u and $\overline{u}$ in the t channel now are in a color octet configuration. Nevertheless, the Odderon calculation serves as a model for the one-gluon exchange contribution as well and its effect on antishadowing.

Acknowledgments: We thank Stefan Kretzer, Kevin McFarlane, and Paul Hoyer for helpful comments, and Alfonso Zerwekh for assistance with the numerical analysis.

References

[1] D. Abbaneo *et al.* [ALEPH Collaboration], arXiv:hep-ex/0112021.

[2] G. P. Zeller *et al.* [NuTeV Collaboration], Phys. Rev. Lett. **88**, 091802 (2002) [Erratum-ibid. **90**, 239902 (2003)] [arXiv:hep-ex/0110059].

[3] P. L. Anthony *et al.* [SLAC E158 Collaboration], Phys. Rev. Lett. **92**, 181602 (2004) [arXiv:hep-ex/0312035].

[4] M. Burkardt and B. Warr, Phys. Rev. D **45**, 958 (1992).

[5] S. J. Brodsky and B. Q. Ma, Phys. Lett. B **381**, 317 (1996) [arXiv:hep-ph/9604393].

[6] S. Kovalenko, I. Schmidt, and J. J. Yang, Phys. Lett. B **546**, 68 (2002).

[7] G. A. Miller and A. W. Thomas, to be published in Int. J. Mod. Phys. E. arXiv:hep-ex/0204007.

[8] G. P. Zeller *et al.* [NuTeV Collaboration], arXiv:hep-ex/0207052.

[9] G. P. Zeller *et al.* [NuTeV Collaboration], Phys. Rev. D **65**, 111103 (2002) [Erratum-ibid. D **67**, 119902 (2003)] [arXiv:hep-ex/0203004].

[10] K. S. McFarland *et al.*, Int. J. Mod. Phys. A **18**, 3841 (2003).

[11] K. P. O. Diener, S. Dittmaier and W. Hollik, Phys. Rev. D **69**, 073005 (2004) [arXiv:hep-ph/0310364].

[12] S. A. Kulagin, Phys. Rev. D **67**, 091301 (2003) [arXiv:hep-ph/0301045].

[13] R. H. Bernstein [NuTeV Collaboration], J. Phys. G **29**, 1919 (2003) [arXiv:hep-ex/0210061].

[14] S. Kretzer, arXiv:hep-ph/0405221.

[15] S. Kretzer *et al.*, Phys. Rev. Lett. **93**, 041802 (2004) [arXiv:hep-ph/0312322].

[16] S. Davidson *et al.*, JHEP **0202**, 037 (2002) [arXiv:hep-ph/0112302].

[17] R. J. Glauber, Phys. Rev. **100**, 242 (1955).

[18] V. N. Gribov, Sov. Phys. JETP **30**, 709 (1970) [Zh. Eksp. Teor. Fiz. **57**, 1306 (1969)].

[19] L. Stodolsky, Phys. Rev. Lett. **18**, 135 (1967).

[20] S. J. Brodsky and J. Pumplin, Phys. Rev. **182**, 1794 (1969).

[21] B. L. Ioffe, Phys. Lett. B **30**, 123 (1969).

[22] L. L. Frankfurt and M. I. Strikman, Nucl. Phys. B **316**, 340 (1989).

[23] B. Z. Kopeliovich, J. Raufeisen and A. V. Tarasov, Phys. Lett. B **440**, 151 (1998) [arXiv: hep-ph/9807211].

[24] D. E. Kharzeev and J. Raufeisen, nucl-th/0206073, and references therein.

[25] A. H. Mueller and A. I. Shoshi, arXiv:hep-ph/0402193.

[26] J. w. Qiu and I. Vitev, arXiv:hep-ph/0405068.

[27] A. D. Martin, M. G. Ryskin and G. Watt, arXiv:hep-ph/0406224.

[28] C. Adloff *et al.* [H1 Collaboration], Z. Phys. C **76**, 613 (1997) [arXiv:hep-ex/9708016].

[29] M. Ruspa, Acta Phys. Polon. B **35**, 473 (2004).

[30] S. J. Brodsky *et al.*, Phys. Rev. D **65**, 114025 (2002) [arXiv:hep-ph/0104291].

[31] S. J. Brodsky, D. S. Hwang and I. Schmidt, Phys. Lett. B **530**, 99 (2002) [arXiv:hep-ph/0201296].

[32] S. J. Brodsky and H. J. Lu, Phys. Rev. Lett. **64**, 1342 (1990).

[33] J. Kuti and V. F. Weisskopf, Phys. Rev. D **4**, 3418 (1971).

[34] M. Arneodo, Phys. Rept. **240**, 301 (1994).

[35] C. Ewerz, arXiv: hep-ph/0306137. See also: H. G. Dosch, C. Ewerz and V. Schatz, Eur. Phys. J. C **24**, 561 (2002) [arXiv:hep-ph/0201294].

[36] J. Bartels, L. N. Lipatov and G. P. Vacca, Phys. Lett. B **477**, 178 (2000) [arXiv: hep-ph/9912423].

[37] P. V. Landshoff, J. C. Polkinghorne and R. D. Short, Nucl. Phys. B **28**, 225 (1971).

[38] S. J. Brodsky, F. E. Close and J. F. Gunion, Phys. Rev. D **8**, 3678 (1973).

[39] L. L. Frankfurt and M. I. Strikman, Nucl. Phys. B **316**, 340 (1988); Phys. Rep. **160**, 235 (1988).

[40] P.D.B. Collins, QCD161:C465, *An Introduction to Regge Theory and High Energy Physics*, (Cambridge University Press) 1977.

[41] V. Barone, C. Pascaud, and F. Zomer, Eur. Phys. J **C 12**, 243 (2000).

[42] CTEQ Collaboration, H. L. Lai, *et al.*, Eur. Phys. J. C **12** (2000) 375.

[43] A. D. Martin *et al.*, Univ. Durham preprint DTP/99/64, hep-ph/9907231 (1999).

[44] New Muon Collaboration, M. Arneodo *et al.*, Nucl. Phys. B **481**, 23 (1996).

[45] New Muon Collaboration, P. Amaudruz *et al.*, Phys. Rev. Lett. **66**, 2712 (1991).

[46] S. Eidelman *et al.* [Particle Data Group Collaboration], Phys. Lett. B **592**, 1 (2004).

[47] EMC-NA28 Collaboration, M. Arneodo *et al.*, Nucl. Phys. B **333**, 1 (1990).

[48] NMC Collaboration, P. Amaudruz *et al.*, Z. Phys. C **51**, 387 (1991).

[49] U. K. Yang *et al.* [CCFR/NuTeV Collaboration], Phys. Rev. Lett. **86**, 2742 (2001) [arXiv:hep-ex/0009041].

[50] K. S. McFarland *et al.*, Nucl. Phys. Proc. Suppl. **112**, 226 (2002).

[51] C. H. Llewellyn Smith, Nucl. Phys. B **228**, 205 (1983).

[52] E. A. Paschos and L. Wolfenstein, Phys. Rev. D **7**, 91 (1973).

[53] E. Leader and E. Predazzi, *An Introduction to gauge theories and the New Physics*, (Cambridge University Press) 1983.

[54] G. P. Zeller, private communication.

[55] J. T. Londergan and A. W. Thomas, Phys. Lett. B **558**, 132 (2003) [arXiv:hep-ph/0301147].

[56] G. R. Farrar, K. Huleihel and H. Y. Zhang, Phys. Rev. Lett. **74**, 650 (1995).

[57] R. Petti, (NOMAD collaboration) presented at ICHEP(2004).

[58] Steve Geer, hep-ph/0210113, Talk given at 4th NuFact '02 Workshop (Neutrino Factories based on Muon Storage Rings), London, England, 1-6 Jul 2002.

[59] S. J. Brodsky, C. R. Ji and G. P. Lepage, Phys. Rev. Lett. **51**, 83 (1983).